Effect of Hydrothermal Temperature on the Structural, Morphological and Optical Properties of Tin Oxide Micro-Flowers

Ali S. Beden[1]* iD ✉ , Hossain M. Moghaddam[2] iD ✉ and Samaneh R. Jamnani [3] iD ✉

[1,2,3]Department of Solid State Physics, Faculty of Basic Sciences, University of Mazandaran, Babolsar, Iran.

*Corresponding author.

Abstract

In the present study, we intend to evaluate the effect of temperature on the structural, morphological, and optical properties of tin oxide. For this purpose, tin oxide micro-flowers were prepared by the hydrothermal method at two different hydrothermal temperatures of 130 and 150°C. The synthesized samples were investigated and characterized using X-Ray Diffraction (XRD), Field Emission Scanning Electron Microscopy (FESEM), Ultraviolet–Visible Spectroscopy (UV-Vis). The XRD results showed that the synthesized samples have single-phase crystallinity with a rutile structure. The mean crystallite size for synthesized Micro- flowers was calculated by the Debby-Scherrer equation and the values were 21 and 28 nm for 130 and 150°C respectively. The results of FESEM showed the morphology of tin oxide is Micro-flower for both temperatures and increasing the temperature from 130 to 150°C caused the morphology of tin oxide samples to change from Micro-flowers consisting of nanoparticles to Micro-flowers consisting of nanoplates. The optical bandgap was increased, whereas the refractive index decreased by increasing temperature from 130 to 150°C.

Keywords: SnO_2, hydrothermal method, optical bandgap.

1. Introduction

Transition metal oxide semiconductors have been the subject of much research because of their applications and properties, such as optical, electrical, magnetic, and electrochemical. Among them, tin oxide is more usable with its unique properties. So, tin oxide (SnO_2) is one of the important metal oxide semiconductors, with a wide energy gap of about 3.6 eV. It is widely used in many fields, such as dye-sensitized solar cells, optical waveguides, gas sensors, transparent conductive electrodes, transistors, and lithium-ion batteries, due to its good chemical stability and excellent electrical and optical properties [1]. The unique structure of this oxide can offer new and promising properties and applications in many fields [2]. Although in all applications, the synthesis of materials with specific morphology and small size, especially in the nanometer dimension, can be an essential factor, so far, physical and chemical methods such as the laser chemical method, chemical precipitation, hydrothermal, and sol-gel have been used to obtain different structures of tin oxide [3-5]. However, the hydrothermal method is a desirable way for the synthesis of tin oxide due to the simplicity of the process, reliability, low cost, as well as the control of morphology and size.

The optical properties of metal oxides are important for many applications, including interference devices such as antireflection coatings, laser mirrors, and monochromatic filters, as well as optoelectronics, optics, solar energy engineering, microelectronics, and optical sensor technology. Therefore, the precise determination of the optical parameters of synthesized products is important in order to understand the mechanism and improve their technology.

So far, nanoparticles of SnO_2 and doped SnO_2 nanostructures have been synthesized by researchers in order to study their structural, morphological, and optical properties. Kumar et al. [6] synthesized tin oxide nanoparticles with different solvent media (water and ethanol) using the co-precipitation method and investigated their optical properties. [7] synthesized tin oxide nanoparticles with the sol-gel method and studied the structural, morphological, and optical properties of the as-synthesized tin oxide nanoparticles calcined at different calcinating temperatures.[8]synthesized tin oxide nanoparticles via the green synthesis method and studied their structural, morphological, and optical properties.[9] synthesized pure and Cd-doped SnO_2 nanostructures with various concentrations of Cd by the hydrothermal method and studied their structural, morphological, and optical properties.

In this research, tin oxide Micro-flowers were synthesized by the hydrothermal method at two different temperatures of 130 and 150 °C, and characterized by XRD, FESEM, and UV-Vis analysis. Then the optical parameters of two samples, such as absorption, transmission percentage, optical bandgap, and refractive index, were investigated and compared.

2. Materials and Methods

For the synthesis of tin oxide first, we dissolved 0.7 grams of Tin (IV) Chloride Pentahydrate $(Sn(Cl_4).5H_2O)$ in 20 ml of deionized water (solution 1). In another container, we dissolved 0.63 grams of sodium hydroxide in 20 ml of deionized water (solution 2). Under rotation, solution 1 was added to solution 2, and the resulting mixture was added to 20 ml of 0.1 M CTAB solution. Then, the solution was transferred to a 100-ml autoclave and put in the furnace at 130 and 150 °C for 32 hours to accomplish hydrothermal procedures. After the natural cooling of the autoclave to room temperature, the precipitate was separated by a centrifuge and washed several times with deionized water and ethanol to remove impurities. Then, it was dried in the oven at 60 °C for 13 hours. Finally, it was calcinated at 400 °C for 4 hours.

3. Results and Discussion

Figure 1 shows the XRD diagram (taken in Beam Gostar Taban Laboratory) of the synthesized samples of tin oxide, which has a rutile structure. The specified peaks are completely consistent with the corresponding reference card number (JCPDS file No. 96-153-4786). The Miller indices related to each angle are specified in **Figure 1**. The sharp and narrow peaks indicate the excellent crystallinity of the two samples. The maximum peak for both samples belongs to the plates with Miller's index (101). With increasing temperature, slight changes in the width and angles of the peaks are observed, as shown in **Figure 2** for three peaks.

The mean crystallite size has been obtained using the Debye-Scherrer formula $D_{hkl} = \frac{0/9\,\lambda}{\beta_{hkl} \cos \theta_{hkl}}$. In this relation, D_{hkl} is the diameter of the nanocrystal, λ is X –ray wavelength $(Cu - K_\alpha \lambda = 1/54\,\text{Å})$، β_{hkl} is full width at half maximum of the diffraction peak in radians, and θ_{hkl} the Bragg angle. The mean size of the nanocrystal for tin oxide synthesized at 130 and 150 °C is 21 and 28 nm, respectively.
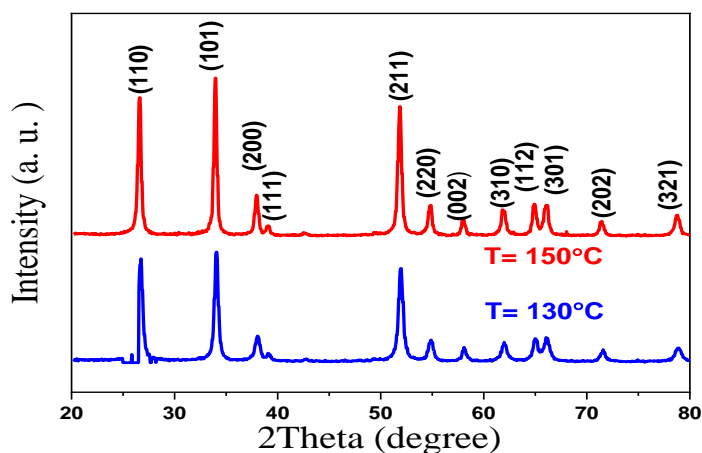
Figure 1. XRD patterns of tin oxide sample synthesized at two temperatures of 130 and 150 ℃.
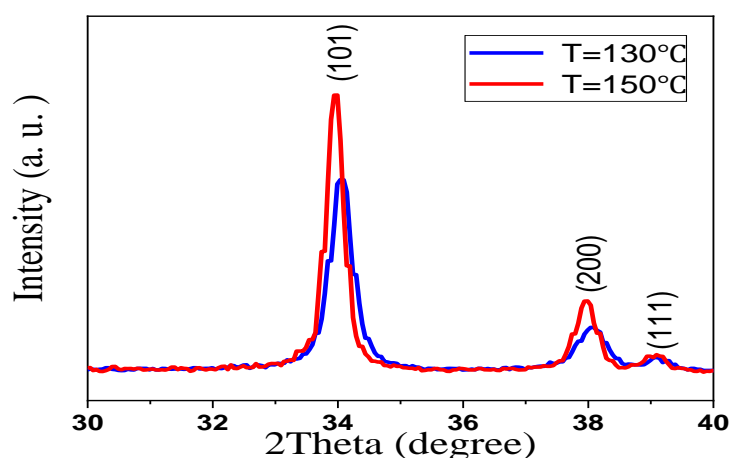
Figure 2. Comparison of XRD peaks of two samples synthesized at 130 and 150 ℃.

FESEM analysis was used to check the morphology of the synthesized samples. **Figure 3** shows the FESEM images of tin oxide synthesized at two hydrothermal temperatures of 130 and 150 ℃. At both temperatures, the morphology includes Micro-flowers. However, the difference is that at the temperature of 130 ℃, tin oxide Micro-flowers contain nanoparticles, whereas when the hydrothermal temperature increases to 150 ℃, the Micro-flowers contain nanoplates.
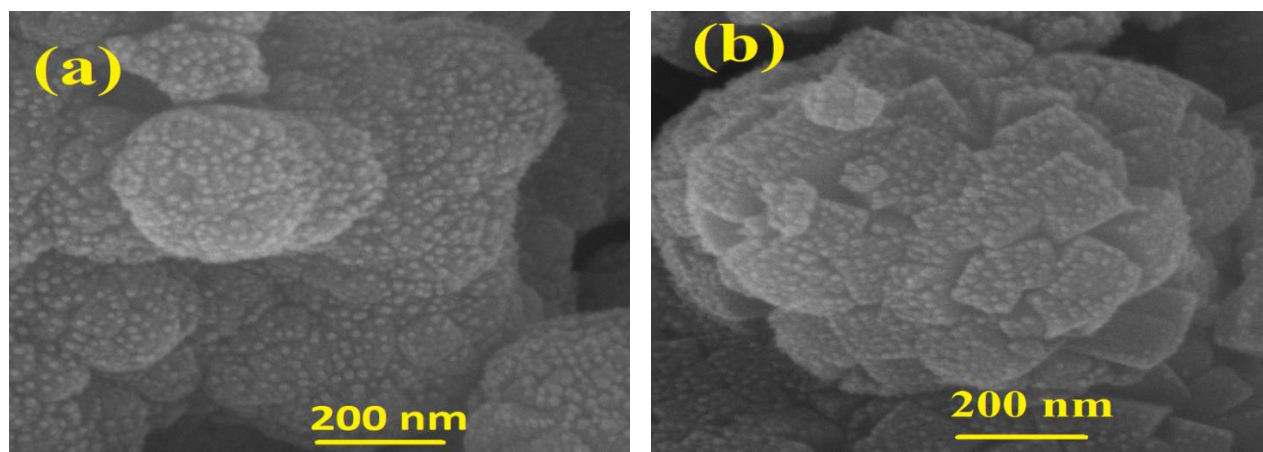
Figure 3. FESEM image of tin oxide synthesized at hydrothermal temperature (a) 130℃ (b) 150℃.

The absorption and transmittance spectra are shown in **Figures 4, 5.** As can be observed, for both samples, the highest value of absorption is in the ultraviolet region. The transmission percentage of the samples is following their absorbance spectra.
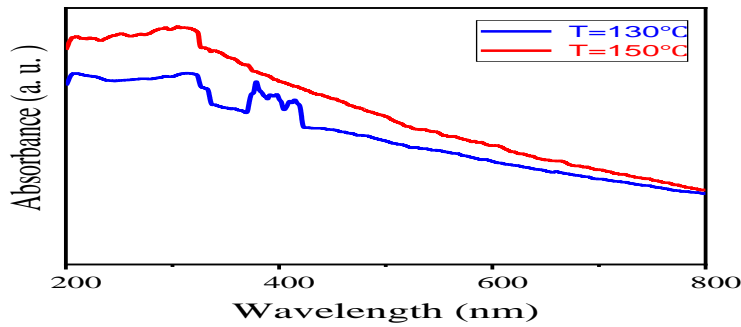
Figure 4. Absorption spectrum of synthesized tin oxide at two temperatures of 130 and 150 ℃.
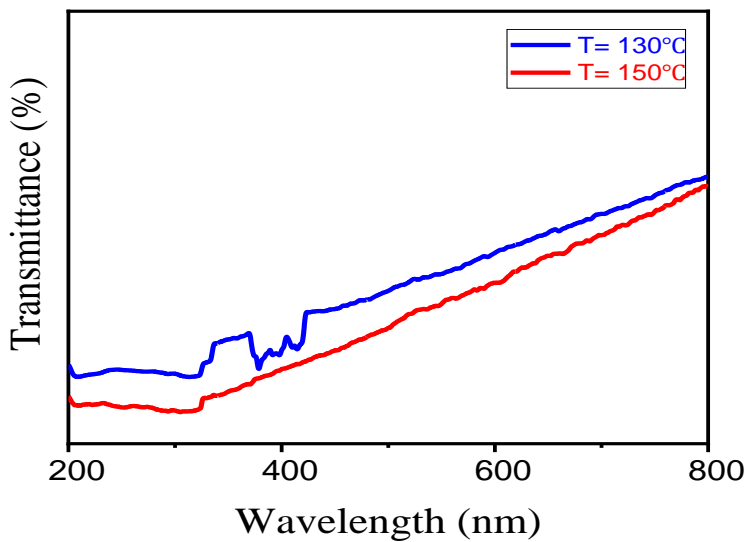
Figure 5. Transmittance spectra of tin oxide passage synthesized at two temperatures of 130 and 150 ℃.

The direct optical bandgap is obtained using Tauc equation [10]:

$$ah\nu = A\left(h\nu - E_g\right)^{1/2} \tag{1}$$

Where α is the absorption coefficient, $h\nu$ is the energy of the incident photon, Eg is the direct optical bandgap, and A is the energy independent constant. $(\alpha h\nu)^2$ is plotted against $h\nu$ in **Figure 6**. The extrapolation of the linear portion of the curve to absorption equal to zero gives the values of the direct band gap. The calculated optical bandgap for tin oxide Micro-flowers is estimated to be around 3.24 and 3.3 eV, which were obtained for temperatures of 130 and 150 ℃, respectively. Considering the temperature difference between the two synthesizes, the optical gap difference is significant at the value of 0.6 electron volts.
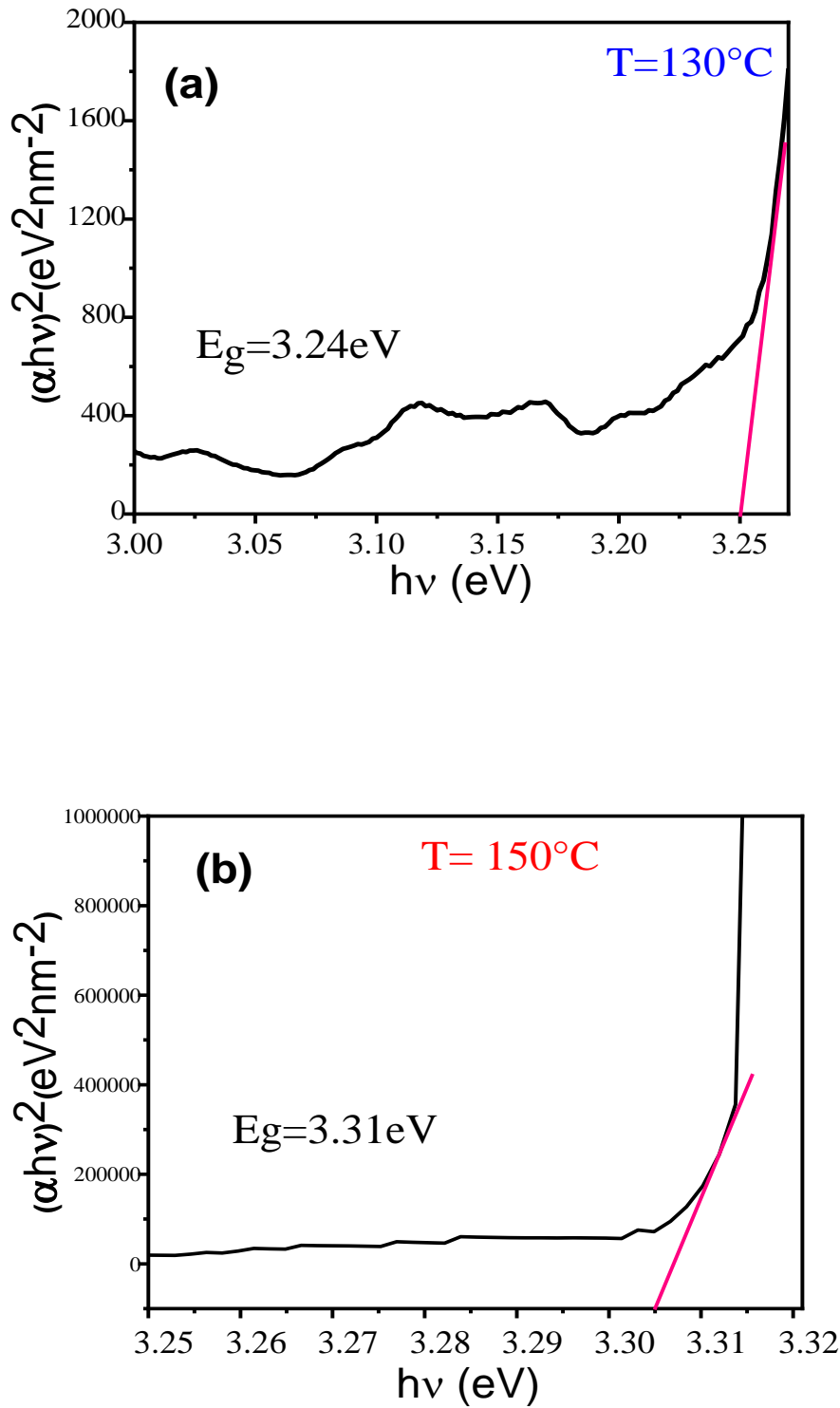
Figure 6. Direct optical bandgap of tin oxide structure synthesized at temperature (a) 130 and (b) 150 ℃.

Absorption, transmittance, reflectivity, and refractive index are examples of optical parameters that quantify how a substance interacts with light. We have applied the following relations for calculating some of the optical parameters, such as reflectivity (R), absorption coefficient (**A**), extinction coefficient (k) and refractive index (n). A is absorption an T is transmittance.

$$R = 1 - A - T \tag{2}$$
$$\alpha = \frac{(1-R)^2}{2R} \tag{3}$$

$$k = \frac{\alpha\lambda}{4\pi} \tag{4}$$

$$R(\lambda) = \frac{(n-1)^2 + k^2}{(n+1)^2 + k^2} \tag{5}$$

Figure 7 shows the changes in refractive index as a function of wavelength for synthesized tin oxides. The value of the refractive index for both samples increases with increasing wavelength, for instance, at the characteristic wavelength of 550 nm, the refractive index has a value of 2.4 and 2.2 for the synthesis temperatures of 130 and 150 ℃, respectively.
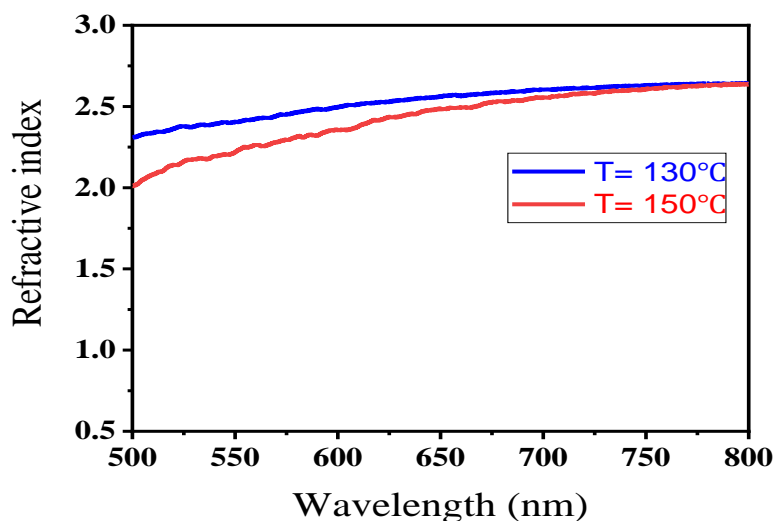
Figure 7. Refractive index diagram (n) of synthesized samples as a function of wavelength.

Refractive index changes in nanostructures depend on the properties of the nanostructures, such as permeability, size, morphology, and distribution of the particles. Since all these factors influence the interaction of incident light with matter, and since this interaction is different from one case to another, different values will be obtained for the refractive index.

4. Conclusion

In this research, tin oxide Micro-flowers were synthesized by the hydrothermal method at two temperatures of 130 and 150 ℃. By increasing the temperature from 130 to 150 ℃, the morphology has changed from Micro-flowers composed of nanoparticles to Micro-flowers composed of nanoplates. While increasing the temperature from 130 to 150 ℃ the mean size of nanocrystals increased, the optical bandgap of tin oxide Micro-flowers increased from 3.24 eV to 3.3 eV, and the refractive index decreased with increasing temperature.

Conflict of Interest

The authors declare that they have no conflicts of interest.

References

1. Jasim, K.E.; Dakhel, A.A. Role of (Cu, Al) codoping in tuning the optical, structural and magnetic properties of Co-doped SnO_2 nanostructures: A comparative study. *Physica B: Condensed Matter* **2021**, *614*, 413040. https://doi.org/10.1016/j.physb.2021.413040.

2. Mahmood, H.; Khan, M.A.; Mohuddin, B.; Iqbal, T. Solution-phase growth of tin oxide (SnO_2) nanostructures: Structural, optical and photocatalytic properties. *Materials Science and Engineering: B* **2020**, *258*, 114568. https://doi.org/10.1016/j.mseb.2020.114568.

3. Matysiak, W.; Tański, T.; Smok, W.; Polishchuk, O.; Synthesis of hybrid amorphous /crystalline SnO_2 1D nanostructures: investigation of morphology, structure and optical properties. *Scientific Reports* **2020,** *10*, 1, 14802. https://doi.org/10.1038/s41598-020-71383-2.

4. Khan, D.; Rehman, A.; Rafiq, M.Z.; Khan, A.M.; Ali, M. Improving the optical properties of SnO_2 nanoparticles through Ni doping by sol-gel technique. *Current Research in Green and Sustainable Chemistry.* **2021**, *4*, 100079. https://doi.org/10.1016/j.arabjc.2017.05.011.

5. Kundu, N.; Jaggi, N.; Synthesis of SnO_2 nano-sheets by hydrothermal route. *In AIP Conference Proceedings* **2020**, *1*, 020049. https://doi.org/10.1063/5.0001708.

6. Kumar, V.; Singh, K.; Kumar, A.; Kumar, M.; Singh, K.; Vij, A.; Thakur, A. Effect of solvent on crystallographic, morphological and optical properties of SnO_2 nanoparticles. *Materials Research Bulletin.* **2017**, *85*, 202-208. https://doi.org/10.4103/0974-620x.116624.

7. Kumar, A.; Chitkara, M.; Dhillon, G. Effect of varying calcination temperature on the structural and optical properties of tin oxide nanoparticles. *Materials Today: Proceedings.* **2023**. *23*, 12-23. https://doi.org/10.1016/j.matpr.2023.05.207.

8. Selvakumari, J.C.; Ahila, M.; Malligavathy, M.; Padiyan, D.P. Structural, morphological, and optical properties of tin (IV) oxide nanoparticles synthesized using Camellia sinensis extract: a green approach. *International Journal of Minerals, Metallurgy, and Materials* **2017**, *24*, 1043-1051. https://doi.org/10.1007/s12613-017-1494-2.

9. Sirohi, K.; Kumar, S.; Singh, V.; Chauhan, N.; Hydrothermal synthesis of Cd-doped SnO_2 nanostructures and their structural, morphological and optical properties. *Materials Today: Proceedings* **2020**, *21*, 1991-1998. https://doi.org/10.1016/j.matpr.2020.01.316.

10. Van Tuan, P.; Hieu, L.T.; Nga, L.Q.; Ha, N.N.; Dung, N.D.; Khiem, T.N.; Influence of Hydrothermal Temperature on the Optical Properties of Er-Doped SnO_2 Nanoparticles. *Journal of Electronic Materials* **2017**, *46*, 3341-3344. https://doi.org/10.1111/j.1365-3156.2006.01562.x.

11. Pazouki, S.; Memarian, N.; Effects of Hydrothermal temperature on the physical properties and anomalous band gap behavior of ultrafine SnO_2 nanoparticles. *Optik.* **2021**, *246*, 167843. https://doi.org/10.1016/j.ijleo.2021.167843

12. Ziegler, J.F.; Biersack, J.P.; Littmark, U. the stopping and range of ions in solids. *Pergamon Press, New York.* **1985**. *12*(*32*), 44-56. https://doi.org/10.1007/978-3-642-68779-2_5.

13. Trim, V.; Ziegler, J.F.; Biersack, J P. Updated version of a computer code for calculating stopping and Ranges, described in *reference*, *Appl. Physics*.**2003**. *12*(*4*), 45-56. https://doi.org/10.1016/J.NIMB.2010.02.091.

14. Bowler, M. Nuclear physics. *Pergamon Press Ltd. Oxford* **1973**, 232.

15. Pupillo, G.; Sounalet, T.; Michel, N.; Mou, L.; Esposito, J.; Haddad, F. New production cross sections for the theranostic radionuclide 67Cu. *Nuclear Instruments and Methods in Physics Research Section B: Beam Interactions with Materials and Atoms.* **2018**, *415*, 41. 23-44.

16. Szelecsenyi, F.; Steyn, G.F.; Methods in Physics Res., Sect. B. *Journal Nuclear. Instrument* **2005,** *234*, 4, 12-34**.**

17. Szelecsenyi, F.; Kovacs, Z. Investigation of direct production of ^{68}Ga with low energy multiparticle accelerator. *Journal Radio-chemica Acta, Germany.* **2012**, *100*, 5, 34-45. https://doi.org/10.1524 /ract .2011.1896

18. Stoll, T.; Kastleiner, S. Excitation functions of proton-induced reactions on 68-Zn from threshold up to 71 MeV, with specific reference to the production of 67-Cu. *Journal Radio-chemical Acta, Germany* **2002**, *l9* (*309*), 33-45. https://doi.org/10.1524/ract.2002.90.6.309.

19. Szelecsenyi, F.; Boothe, T.E.; Takacs, S. Evaluation of direct production of Ga with high energy multiparticle. *Journal Applied Radiation and Isotopes*, **1998**, *49*, 1005, 45-65. https://doi.org/10.1016/S0969-8043%2897%2910103-8.

20. Hermanne, A. Evaluated cross-section and thick target yield databases of Zn+p processes for practical applications. *Journal Applied Radiation and Isotopes* **1997**, *49*(1005), 23-33. https://doi.org/10.1016/S0969-8043(97)10103-8.

21. Norton, K.J.; Firoz, A.; David, J.L.; A review of the synthesis, properties, and applications of bulk and two-dimensional tin (II) sulfide (SnS). *Applied Sciences* **2021,** *11*, 5, 2062. https://doi.org/10.3390/app11052062.

22. Yu, J.; Yingeng, W.; Yan, H.; Xiuwen, W.; Jing, G.; Jingkai, Y.; Hongli, Z. Structural and electronic properties of SnO$_2$ doped with non-metal elements. *Beilstein Journal of Nanotechnology* **2020,** *11*(*1*), 1321-1328. https://doi.org/10.3762/bjnano.11.116.

23. Pargoletti, E.; Umme, H.H.; Iolanda, D.B.; Hongjun, C.; Thanh, T.P.; Gian, L.; Chiarello, J.; Lipton, D.; Valentina, P.; Antonio, T.; Giuseppe, C. Engineering of SnO$_2$–graphene oxide nano heterojunctions for selective room-temperature chemical sensing and optoelectronic devices. *ACS Applied Materials & interfaces* **2020,** *12*(*35*), 39549-39560. https://doi.org/10.1021/acsami.0c09178.

24. Wang, B.; Zhu, L.F.; Yang, Y.H.; Xu, N.S.; Yang, G.W. Fabrication of a SnO2 nanowire gas sensor and sensor performance for hydrogen. *The Journal of Physical Chemistry C.* **2008,** *112*(*17*), 6643-6647. https://doi.org/10.1021/jp8003147.

25. Das, S.; Jayaraman, V. SnO$_2$: A comprehensive review on structures and gas sensors." *Progress in Materials Science* **2014,** *66,* 112-255. https://doi.org/10.1016/j.pmatsci. 2014.06.003.

26. Castro, A.; Marques, M.A.; Rubio, A. Propagators for the time-dependent Kohn–Sham equations. *The Journal of Chemical Physics* **2004**, *121*(*8*), 3425-33. https://doi.org/10. 1063/1.1774980.

27. Brockherde, F.; Vogt, L.; Li, L.; Tuckerman, M.E.; Burke, K.; Müller. K.R. Bypassing the Kohn-Sham equations with machine learning. *Nature Communications* **2017**, *8*(*1*), 872. https://doi.org/10.1038/s41467-017-00839-3.

28. Sahoo, L.; Bhuyan, S.; Das, S.N. Structural, morphological, and impedance spectroscopy of Tin oxide-Titania based electronic material. *Physica B: Condensed Matter* **2023,** 654, 414705. https://doi.org/10.1016/j.physb.2023.414705.

29. Tui, R.; Sui, H.; Mao, J.; Sun, X.; Chen, H.; Duan, Y.; Yang, P.; Tang, Q.; He, B. Round-comb Fe$_2$O$_3$& SnO$_2$ heterostructures enable efficient light harvesting and charge extraction for high-performance all-inorganic perovskite solar cells. *Journal of Colloid and Interface Science* **2023**, *15*(640), 18-27. https://doi.org/10.1016/j.jcis.2023.03.034.

30. Du, B.; Kun, He.; Gangqi, T.; Xiang, C.; Lin, S. Robust Electron Transport Layer of SnO$_2$ for Efficient Perovskite Solar Cells: Recent Advances and Perspectives. *Journal of Materials Chemistry C.* **2023**, *12*, 3, http://dx.doi.org/10.1016/j.optmat.2023.113518.